Microstructure of bilayer manganite $PrCa_2Mn_2O_7$ showing charge/orbital ordering

Zhanbing He,[1,a)] He Tian,[1] Guochu Deng,[2,3] Qiang Xu,[1,4] and Gustaaf Van Tendeloo[1]

[1]*Electron Microscopy for Materials Research (EMAT), University of Antwerp, Groenenborgerlaan 171, Antwerp B-2020, Belgium*
[2]*Laboratory for Developments and Methods, Paul Scherrer Institute, CH-5232 Villigen, Switzerland*
[3]*Bragg Institute, Australian Nuclear Science and Technology Organization, New Illawarra Road, Lucas Heights, NSW 2234, Australia*
[4]*National Centre for High Resolution Electron Microscopy, Technical University Delft, Lorentzweg 1, 2628 CJ Delft, The Netherlands*

The microstructure of the charge/orbital ordering Ruddleden-Popper phase $PrCa_2Mn_2O_7$ was studied by transmission electron microscopy along both the [001] and the [110] orientation. Three coexisting charge/orbital ordering phases CO1, CO2, and CO3 were observed along the [001] orientation at room temperature. Different from the one-dimensional modulation in the CO1 and CO2 phase, the CO3 phase is characterized by two sets of mutually perpendicular structural modulations. From [110] high angle annular dark field-scanning transmission electron microscopy, we found that the Pr atoms locate in-between the bilayer MnO_6 octahedra, which is different from the previous reports. © 2013 AIP Publishing LLC. [http://dx.doi.org/10.1063/1.4807758]

The strongly correlated electronic systems of perovskite manganites have received great attention because of their fascinating physical properties such as colossal magnetoresistance and high spin polarity, which could find potential applications in spintronics or magnetic tunnel junction.[1–9] The physical mechanism of these properties was ascribed to the complicated interplays between the four degrees of freedom of lattice, charge, orbital, and spin, and the consequent ordering as well as possible phase separation.[6,10–12]

Recently, two distinct charge/orbital ordering (CO/OO) states were found in the Ruddlesden-Popper (RP) compound $Pr(Sr_{1-x}Ca_x)_2Mn_2O_7$.[13] $Pr(Sr_{1-x}Ca_x)_2Mn_2O_7$ has a layer structure (AO) $(ABO_3)_n$ $(n=2)$, where two (ABO_3) perovskite layers are separated by a AO rock salt layer along the long axis. The two reported CO/OO phases in $Pr(Sr_{0.1}Ca_{0.9})_2Mn_2O_7$ are the high-temperature phase CO1 phase at $330\,K > T > 295\,K$ (lattice parameters $a = 0.5412$, $b = 1.0921$, $c = 1.9234$ nm, and space group $Pbnm$) and the lower-temperature CO2 phase at $T < 295\,K$ ($a = 1.0812$, $b = 0.5475$, $c = 1.9203$ nm, and space group $Am2m$, Ref. 13). The CO1 phase is centrosymmetric without any spontaneous electric polarization, but the CO2 phase is a noncentrosymmetric phase with spontaneous electric polarization.[13] The thermally induced rotation of orbital stripes between these two ordering phases has attracted extensive interest.[14–18] However, the limited information about its microstructures has obstructed a better understanding of the macro properties and physics underneath. Therefore, we carried out a transmission electron microscopy (TEM) study on $PrCa_2Mn_2O_7$ to reveal the different aspects of the microstructure. The phases and micro domains viewed along the [001] zone axis are discussed. The heavy Pr atoms were found to locate in-between the bilayer MnO_6 octahedra.

Bulk $PrCa_2Mn_2O_7$ samples were synthesized using a traveling solvent floating zone method with high oxygen background pressure.[17,18] Powdered samples, deposited on a Cu grid coated with a holey carbon film, as well as Ar-ion milled TEM samples were used for TEM investigation. A Tecnai G^2 electron microscope equipped with a Gatan cooling and heating holder operated at 200 kV was used to record electron diffraction (ED) patterns, high resolution TEM (HRTEM) images, and carry out *in situ* TEM observations. High angle annular dark field-scanning TEM (HAADF-STEM) was performed on the Qu-Ant-EM (FEI Titan 80-300 "cubed") microscope, with aberration-correctors for both probe-forming and imaging lenses. We used STEMSIM software to perform STEM simulation. For these simulations, the thickness of the sample is chosen as 20 nm and the same detector configuration (50 mrad inner and 115 mrad outer angle of the HAADF detector) as in the experiments.

The CO/OO phenomenon was observed along the [001] direction by the appearance of satellite spots for both the CO1 and CO2 phase.[14] Therefore, it is particularly important to reveal the microstructure along this direction. Fig. 1(a) is a typical bright-field image at room temperature taken along the [001] orientation; several domains are clearly present. The CO1/CO2 phases and crystallographic orientation (as marked) in different domains are deduced from the selected-area ED patterns, insetted in the schematic diagram in Fig. 1(b). The orientation of the orbital stripes in different domains is schematically illustrated by heavy arrows according to the orientation of the lines of satellite spots found in the ED patterns. Clamped by the A and F domain, domains from B to E have the same height and are well aligned from left to right. Different from the common straight domain boundaries in this system, the domain boundary between the domains C and D is curved, as marked by some small dots. The phases in A, B, C, F, and G exhibit the CO1 phase, which is a high temperature phase in the previous reports,[13,14] but a room temperature

a)Author to whom correspondence should be addressed. Electronic addresses: Zhanbing.He@ua.ac.be and hezhanbing@gmail.com
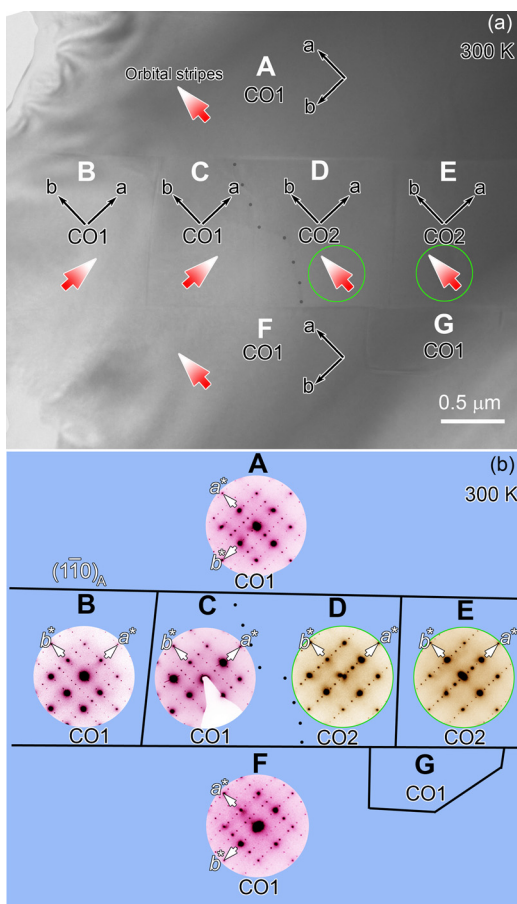
FIG. 1. (a) CO1 and CO2 domains at room temperature viewed along the [001] direction. The phases and crystallographic orientations in each domain were determined by the ED patterns (insetted in (b)). The heavy arrows indicate the expanding direction of the zigzag orbital stripes. (b) Schematic diagram of the domains in (a). The selected-area ED patterns are insetted in each domain.

FIG. 2. (a) $[00\text{-}1]_{CO1}$ HRTEM image of a (110) twin. (b) A phase boundary between two crystal grains of the CO1 phase. (c) and (d) FFT of the HRTEM images from one single CO1 grain, and from two crystal grains, respectively. Note that the split of diffraction spots in (d) indicates a small rotation of the planes in both grains.

phase in our samples. The CO2 phase in the D and E domains has almost the same crystallographic orientation, similar to that of the CO1 phase in the B and C domains.

The domain boundary between B and A (or F) is deduced as $(1\text{-}10)_A$ and the crystallographic orientation between them is rotated by $\sim 90°$ around the [001] axis, as deduced from ED patterns, implying a $(1\text{-}10)_A$ twin relationship between them. The twin domains were believed to be caused by the phase transition from the parent phase with a higher symmetry[19] and generally generates a splitting of some diffraction spots in the [001] zone axis.[20,21] The [00-1] HRTEM image in Fig. 2(a) further reveals the characteristics of this kind of twin. The two adjacent domains are connected with each other through the $(1\text{-}10)_A$ twin boundary (TB). The lattice fringes with a width of 0.54 nm (corresponding to the magnitude of a_{CO1}) are nearly perpendicular to each other in both domains. A careful measurement, however, indicates that the angle between both b axes in the two domains is not exactly 90°, but different by 0.9° (as shown by the thin white and black lines).

The crystallographic orientation between domains B and C is almost the same, as seen from their similar orientation of their [001] ED patterns in Fig. 1(b). A slight difference, however, is found from the fast Fourier transform (FFT) (Fig. 2(d)) of the HRTEM image including B and C domain
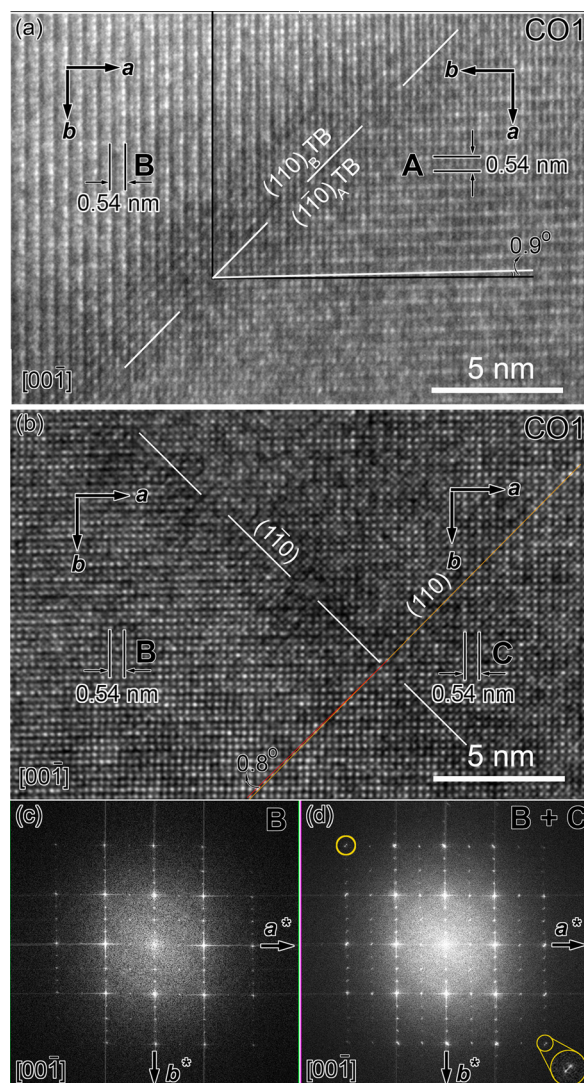
boundaries (Fig. 2(b)). Compared to the FFT of the HRTEM image from one single domain (Fig. 2(c)), some of the high-index diffraction spots in Fig. 2(d) are evidently split, e.g., the (h h 0) spots in the red circles, suggesting a small rotation of the lattice around the [001] axis occurred in the adjacent B and C domains, e.g., 0.8° deviation for the (110) plane in both domains, the same as that deduced from the split of the diffraction spots in the red circles.

In order to study the change of domains and orbital stripes when the CO2 phase is clamped by the CO1 phase, we carried out an *in situ* heating TEM experiment. Fig. 3(a) is the bright-field TEM image of the areas in Fig. 1(a), but taken at 333 K. The mass loss during the *in situ* observation can be ignored because the sample is stable in that range of temperatures. All phases in each domain are determined as CO1 by selected-area ED patterns, as indicated in Fig. 3(b). The thermally induced 90° rotation of the orbital stripes was observed only in the domains D and E (highlighted by green circles), as revealed by the 90° rotation of the lines of satellite spots in their [001] ED patterns, in agreement with
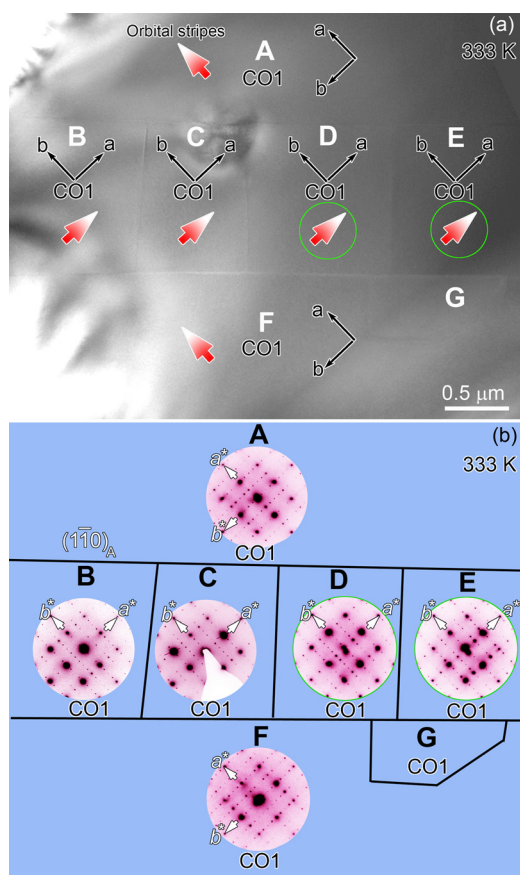
FIG. 3. (a) The domain configuration at 333 K compared to that at room temperature in Fig. 1(a). (b) Schematic diagram of the domains in (a). Note that the direction of the orbital stripes of the CO2 phase at room temperature (as emphasized using green circles) was changed by 90° upon heating, accompanying the phase change from CO2 to CO1.
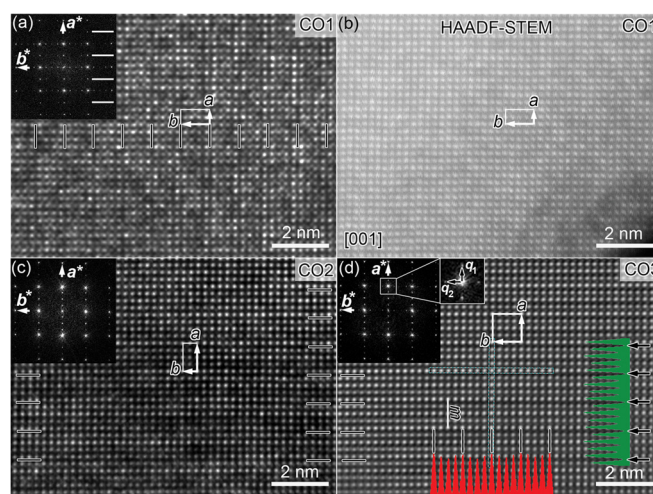

FIG. 4. (a) [001] HRTEM image of the CO1 phase; (b) [001] HAADF-STEM image of the CO1 phase; (c) [001] HRTEM image of the CO2 phase. Note that the difference of the CO1 and CO2 phase is easily found from the insetted FFT image because of the different space groups. (d) [001] HRTEM image of the CO3 phase. The two modulations along vertical and horizontal direction can be seen from both the insetted intensity profile and FFT. However, the difference of the red and green intensity profile insetted in (d) implies that the two modulations come from varying origins.

previously observations.[13,21,22] However, the orientation of the orbital stripes of the CO1 phase is conserved during the increase of temperature. Consequently, all the domains are the CO1 phase and the orientation of both orbital stripes and lattice from B to E is nearly the same. The twin relationship between B (or C, D, E) and A (or F) domains is also the same as that of the B and A domains at room temperature. Furthermore, the straight boundaries between them are maintained and domains from B to E are still clamped by A and F. However, the curved boundary between C and D domains in Fig. 1(a) disappeared and is replaced by a straight boundary after the phase transition. The disappearance of the curved boundary between C and D implies its lower energy.

HRTEM image is a widely used technique to analyze the microstructure of perovskite-based manganites, and CO/OO stripes.[23–35] Fig. 4(a) is a [001] HRTEM image of the CO1 phase. The stripes of CO/OO with a modulation period of 1.08 nm are running along the b-direction, as marked by short line segments. The intensity of the bright spots in the HAADF-STEM image of Fig. 4(b) is constant and homogeneous, implying the superlattice is not caused by A-site cation ordering, concordant with the observation in $Pr_{0.5}Ca_{0.5}MnO_3$,[30] but different from the observed A-site cation ordering in $La_{0.75}Ca_{0.25}MnO_3$.[36] Fig. 4(c) is a [001] HRTEM image of the CO2 phase, where the superlattice with a period of ∼1.08 nm runs along the a-direction. It is difficult to distinguish between the CO1 and CO2 phase

from [001] HRTEM images because they have similar structure blocks and modulation period. However, the difference is clearly seen from the insetted FFT of the HRTEM images. Comparing to the FFT of the CO2 phase in Fig. 4(c), there is one more line of weak spots in-between the lines of the main diffraction spots for the CO1 phase, as indicated by short white segments in the insetted FFT image in Fig. 4(a).

In addition to the CO1 and CO2 phase, the third CO/OO phase with two orthogonal modulations, named CO3, is also found at room temperature, as seen in Fig. 4(d). After carefully checking the $[001]_{CO2}$ HRTEM images, some areas show two sets of mutually perpendicular structural modulations, also verified by the satellite spots with two modulation vectors $q_1 = 1/2\ a_0^*$, and $q_2 = 1/2\ b_0^*$, as clearly seen from the FFT insetted in Fig. 4(d). The two superlattices in the HRTEM image, along the vertical and horizontal directions, respectively, have almost the same period of ∼1.08 nm, equal to that of b_{CO1} (or a_{CO2}). The intensity of line scans along two perpendicular directions in the middle of Fig. 4(d) shows the difference of the two sets of superlattices. On the one hand, the intensity of the red profile from the horizontal atomic line shown in the bottom has a higher symmetry than the green one from the vertical atomic line in the right part. A mirror m perpendicular to the b-axis within one superlattice period could be deduced from the red profile, while no mirror could be found in the green profile. On the other hand, the deeper grooves in the green profile (as indicated by arrows at the right part) were arranged periodically along the a-axis, while no periodically darker contrast was found along the b-direction (see the red profile). The difference of intensity profile of the two sets of superlattice could be caused by various origins[37–39] and the reasons need to be further clarified. More importantly, the CO3 phase might be an intermediate state of the 90° rotation of the OO stripes between the phase transition of the CO1 and CO2 phase, as observed by the ED patterns with two perpendicular modulations.[21]
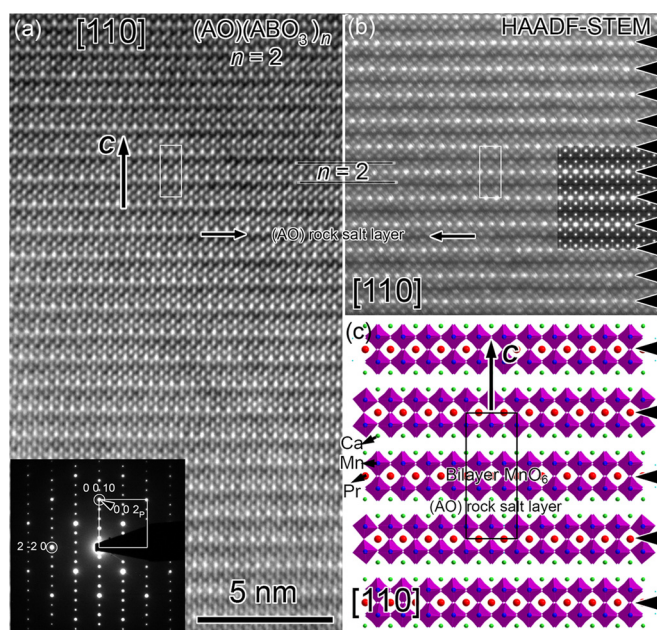
FIG. 5. (a) [110] HRTEM image of $PrCa_2Mn_2O_7$ with the $n = 2$ RP structure, showing a perfect stacking of layers along the c axis. The [110] ED pattern is insetted. (b) The HAADF-STEM image demonstrates that the white dots (corresponding to heavy Pr atoms) locate in-between the bilayer of MnO_6 octahedra, as evidenced by the structure model in (c). The insetted simulated HAADF-STEM image at the right of (b) is in good agreement with the experimental results.

The bilayer structure of $PrCa_2Mn_2O_7$ is demonstrated from observations along the [110] orientation. The [110] HRTEM image in Fig. 5(a) shows the alternating bilayer MnO_6 octahedron blocks and the AO rock salt layer stacking along the c axis, indicating a well-ordered $n = 2$ RP structure, quite similar to the structure projection of $Ca_3Mn_2O_7$ (with a similar unit cell) along the same direction.[28] The number n of (AO) $(ABO_3)_n$, namely, the perovskite thickness, could be also determined directly from ED patterns containing $c*$ as $n = N/2$, where N is the number of diffraction spots between the central spot and the $(002)p$ reflection of cubic perovskite.[24] The $n = 2$ is found from the [110] ED pattern insetted in Fig. 5(a) because of 4 spots between the central spot and $(002)p$. No diffuse scattering along $c*$ was found, suggesting a perfect stacking along the c-direction. The [110] HAADF-STEM image in Fig. 5(b) is characterized by whiter spots arranged in line (emphasized by arrows in the right) and located in the middle of the two adjacent dark lines (rock salt layers), implying that the heavy Pr atoms (the whiter spots) locate in-between the bilayer MnO_6 layers, which is not concordant with the results by X-ray diffraction.[13,40] A structural model of $PrCa_2Mn_2O_7$ with Pr atoms only located in-between the bilayer MnO_6 layers is therefore proposed in Fig. 5(c). The simulated HAADF-STEM image based on this model (as insetted in the right of Fig. 5(b)) shows a good agreement with the experimental results, in contrast to the disordered phase of $Pr(Ca_{0.9}Sr_{0.1})_2Mn_2O_7$,[40] where both Ca and Pr atoms locate at the cages of the MnO_6 octahedra and also in the AO layers.

In summary, the microstructure of the CO/OO Ruddleden-Popper bilayer manganite $PrCa_2Mn_2O_7$ was studied by electron microscopy along both [001] and [110] zone axes. Three CO/OO phases, namely CO1, CO2, and CO3, were found to coexist at room temperature, where the CO3 phase has two orthogonal superlattices with a similar modulation period of 1.08 nm along the a and b axis, respectively. The *in situ* heating TEM experiment indicates that the CO2 phase, clamped by the CO1 domains, can change into the CO1 phase by heating, inducing a 90° rotation of the OO stripes. A perfect bilayer MnO_6 perovskite block stacking along the c axis is observed along the [110] orientation. However, the Pr atoms were found to locate in-between the bilayer MnO_6 octahedra from [110] HAADF-STEM image and simulation, which is different from previous reports from X-ray diffraction.

[1]C. N. R. Rao, A. K. Cheetham, and R. Mahesh, Chem. Mater. **8**, 2421 (1996).

[2]A. P. Ramirez, J. Phys.: Condens. Matter **9**, 8171 (1997).

[3]M. Imada, A. Fujimori, and Y. Tokura, Rev. Mod. Phys. **70**, 1039 (1998).

[4]J. M. D. Coey, M. Viret, and S. von Molnar, Adv. Phys. **48**, 167 (1999).

[5]Y. Tokura and Y. Tomioka, J. Magn. Magn. Mater. **200**, 1 (1999).

[6]E. Dagotto, T. Hotta, and A. Moreo, Phys. Rep. **344**, 1 (2001).

[7]Y. Tokura, Phys. Today **56**(7), 50 (2003).

[8]Y. Tokura and N. Nagaosa, Science **288**, 462 (2000).

[9]Y. Tokura, Rep. Prog. Phys. **69**, 797 (2006).

[10]C. N. R. Rao and A. K. Cheetham, Science **276**, 911 (1997).

[11]S. Mori, C. H. Chen, and S.-W. Cheong, Nature **392**, 473 (1998).

[12]E. Dagotto, Science **309**, 257 (2005).

[13]Y. Tokunaga, T. Lottermoser, Y. Lee, R. Kumai, M. Uchida, T. Arima, and Y. Tokura, Nature Mater. **5**, 937 (2006).

[14]Y. Tokunaga, T. J. Sato, M. Uchida, R. Kumai, Y. Matsui, T. Arima, and Y. Tokura, Phys. Rev. B **77**, 064428 (2008).

[15]T. A. W. Beale, S. R. Bland, R. D. Johnson, P. D. Hatton, J. C. Cezar, S. S. Dhesi, M. v. Zimmermann, D. Prabhakaran, and A. T. Boothroyd, Phys. Rev. B **79**, 054433 (2009).

[16]H. Itoh, Y. Tokunaga, N. Kida, R. Shimano, and Y. Tokura, Appl. Phys. Lett. **96**, 032902 (2010).

[17]R. Thiyagarajan, G. Deng, S. Arumugam, D. Mohan Radheep, U. Devarajan, A. Murugeswari, P. Mandal, E. Pomjakushina, and K. Conder, J. Appl. Phys. **110**, 093905 (2011).

[18]G. Deng, R. Thiyagarajan, D. Mohan Radheep, E. Pomjakushina, M. Medarde, A. Krzton-Maziopa, S. Wang, S. Arumugam, and K. Conder, J. Cryst. Growth **353**, 25 (2012).

[19]G. Van Tendeloo and S. Amelinckx, Acta Crystallogr., Sect. A **30**, 431 (1974).

[20]Y. Wang, F. Guyot, and R. C. Liebermann, J. Geophys. Res. **97**, 12327, doi:10.1029/92JB00870 (1992).

[21]Z. He, G. Deng, H. Tian, Q. Xu, and G. Van Tendeloo, J. Solid State Chem. **200**, 287 (2013).

[22]Z. A. Li, X. Li, Z. Wang, H. F. Tian, C. Ma, L. J. Zeng, and H. X. Yang, EPL **86**, 67010 (2009).

[23]L. A. Bendersky, R. Chen, I. D. Fawcett, and M. Greenblatt, J. Solid State Chem. **157**, 309 (2001).

[24]R. Chen, M. Greenblatt, and L. A. Bendersky, Chem. Mater. **13**, 4094 (2001).

[25]C. Autret, R. Retoux, M. Hervieu, and B. Raveau, Chem. Mater. **13**, 4745–4752 (2001).

[26]R. Wang, J. Gui, Y. Zhu, and A. R. Moodenbaugh, Phys. Rev. B **63**, 144106 (2001).

[27]Y. Q. Wang, X. F. Duan, Z. H. Wang, J. R. Sun, and B. G. Shen, Appl. Phys. Lett. **78**, 2479 (2001).

[28]L. A. Bendersky, M. Greenblatt, and R. Chen, J. Solid State Chem. **174**, 418 (2003).

[29]M. Giot, P. Beran, O. Perez, S. Malo, M. Hervieu, B. Raveau, M. Nevriva, K. Knizek, and P. Roussel, Chem. Mater. **18**, 3225 (2006).

[30]L. Wu, R. F. Klie, Y. Zhu, and Ch. Jooss, Phys. Rev. B **76**, 174210 (2007).

[31]Y. Wang and R. Yu, Phys. Status Solidi A **206**, 31 (2009).

[32]H. X. Yang, H. F. Tian, Y. J. Song, Y. B. Qin, Y. G. Zhao, C. Ma, and J. Q. Li, Phys. Rev. Lett. **106**, 016406 (2011).

[33]T. W. Eom, Y. H. Hyun, J. S. Park, Y. P. Lee, V. G. Prokhorov, V. S. Flis, and V. L. Svetchnikov, Appl. Phys. Lett. **94**, 152502 (2009).

[34]J. C. Loudon, L. Fitting Kourkoutis, J. S. Ahn, C. L. Zhang, S.-W. Cheong, and D. A. Muller, Phys. Rev. Lett. **99**, 237205 (2007).

[35]J. Hadermann, A. M. Abakumov, T. Perkisas, H. D'Hondt, H. Tan, J. Verbeeck, V. P. Filonenko, E. V. Antipov, and G. Van Tendeloo, J. Solid State Chem. **183**, 2190–2195 (2010).

[36]V. Moshnyaga, L. Sudheendra, O. I. Lebedev, S. A. Koster, K. Gehrke, O. Shapoval, A. Belenchuk, B. Damaschke, G. van Tendeloo, and K. Samwer, Phys. Rev. Lett. **97**, 107205 (2006).

[37]A. Arulra, P. N. Santhosh, R. S. Gopalan, A. Guha, A. K. Raychaudhuri, N. Kumar, and C. N. R. Rao, J. Phys.: Condens. Matter **10**, 8497 (1998).

[38]F. Rivadulla, E. Winkler, J.-S. Zhou, and J. B. Goodenough, Phys. Rev. B **66**, 174432 (2002).

[39]M. W. Lufaso and P. M. Woodward, Acta Crystallogr., Sect. B **60**, 10 (2004).

[40]D. Okuyama, Y. Tokunaga, R. Kumai, Y. Taguchi, T. Arima, and Y. Tokura, Phys. Rev. B **80**, 064402 (2009).